ACCEPTED MANUSCRIPT
The Journal of Chemical Physics
AIP Publishing
This is the author's peer reviewed, accepted manuscript. However, the online version of record will be different from this version once it has been copyedited and typeset.
PLEASE CITE THIS ARTICLE AS DOI: 10.1063/5.0319029

Pump–Probe Fluorescence Lifetime Imaging Microscopy

Malcolm Garrow[1], Adil Haboucha[2], Petr Heřman[1], Pavel Malý[1*]

1 Faculty of Mathematics and Physics, Institute of Physics, Charles University, Prague, Czech Republic

[2] Photonics Bretagne, Lannion, France

**pavel.maly@matfyz.cuni.cz*

Abstract

Pump–probe spectroscopy is the most popular technique to resolve ultrafast photo-induced dynamics. Its fluorescence-detected variant connects it to fluorescence microscopy, for a combined spatial and temporal resolution in sensitive samples. In this work, we introduce fluorescence-detected pump–probe spectroscopy (F-PP) with fluorescence lifetime imaging microscopy (FLIM) detection, that we call pump–probe FLIM (PP-FLIM). Like FLIM, PP-FLIM images the time-resolved fluorescence decay in three spatial dimensions. At each voxel, furthermore, the full pump–probe spectrum is obtained, measuring spectrally resolved transient dynamics. We demonstrate the PP-FLIM principle on microliter-volume mixture of two fluorescent dyes, oxonol VI and cresyl violet, whose transient spectra PP-FLIM disentangles by their fluorescence lifetime. We then showcase the high-resolution non-invasive ultrafast imaging by measurement of individual chloroplasts within intact spinach leaves.

I. INTRODUCTION

Pump–probe (PP) spectroscopy is possibly the most common technique of detecting ultrafast photophysical and photochemical processes in a large variety of systems. This technique works by using two short laser pulses: the first, called the "pump," excites the sample whilst the second, the "probe," allows for the observation of the photodynamics taking place within the system after a time delay. Commonly used spectroscopic PP experiments include photoelectron[1–3] (for gas phase samples) and transient absorption (TA)[4–6] (for samples in the solution or solid phases). These methods have proven to be powerful in a wide variety of chemical physics applications, such as determining the dynamics of photocatalysts,[7,8] photoactive materials,[9,10] and in energy and charge transfer.[11–14] Structures of excited state species[15–17] and mechanisms of photochemical reactions[18,19] have also been studied using ultrafast PP spectroscopy. As with any experimental technique, standard transient absorption has its limitations. These include detection of small changes against the bright background of the probe light, complicating its application to samples with low optical density that give a low transient signal. Furthermore, off-resonant coherent artifacts such as cross-phase modulation and solvent response can obscure the sample dynamics on the femtosecond timescale.[20–22] In its microscopy application, TA faces additional challenges in form of sample photobleaching and degradation, small relative transient signal from the small probed volume, long data

ACCEPTED MANUSCRIPT
The Journal of Chemical Physics
AIP Publishing
This is the author's peer reviewed, accepted manuscript. However, the online version of record will be different from this version once it has been copyedited and typeset.
PLEASE CITE THIS ARTICLE AS DOI: 10.1063/5.0319029

acquisition times, restriction to transparent samples, and a difficulty of separating the pump and probe pulses in detection.[23,24]

Variants of pump–probe spectroscopy have been developed to lift or circumvent these limitations. Among these, we have recently introduced fluorescence-detected PP spectroscopy (F-PP)[25], with several works to follow.[26,27] In F-PP, the fluorescence emitted from a sample can easily be separated from the probe light both spectrally and spatially, allowing for detection against a dark background. This also allows for lower laser fluences to be used, so problems with photobleaching and photodamage can be effectively mitigated. This opens up possibilities for fluorescence PP microscopy to image and characterize heterosystems and fragile photoactive systems that transient absorption microscopy would struggle with. There are also no coherent artifacts present in the measured data, allowing for an easier analysis of dynamical processes within the sample. F-PP can be seen as a variant of two-dimensional electronic spectroscopy[28] with fluorescence detection (F-2DES) .[29–32] However, F-2DES requires two pairs of pulses with scanned interferometric delays and an additional phase modulation to separate the nonlinear signal from linear fluorescence, making it significantly more complex instrumentally. Important for microscopy, the measurement time of F-2DES is also at least an order-of-magnitude longer than that of F-PP. In some aspects, the F-PP thus seems to be an optimal variant of PP for microscopy.

Similar to the standing of PP spectroscopy among time-resolved techniques, fluorescence microscopy is the standard workhorse of optical imaging. With its sensitivity, non-invasive character, and versatility, it is the method of choice in physical, chemical, biological and life sciences.[33–35] Among the broad family of fluorescence imaging techniques, fluorescence lifetime imaging microscopy (FLIM) stands out as it provides additional information about the excitation lifetime of the emitting species.[34–36] The excitation lifetime is a robust property of the emitting chromophores, reporting on their local environment and interaction. One major application of FLIM is the detection of Förster resonance energy transfer (FRET) to discern protein interaction in cells.[37,38]

FLIM, as well as variants of PP spectroscopy, are established techniques with a broad scope of application. In this work, we combine F-PP with FLIM, into a technique that we call PP-FLIM, pump–probe fluorescence lifetime imaging microscopy. Like F-PP, PP-FLIM uses a pump pulse to excite the sample and a subsequent probe pulse pair to track the ultrafast photo-induced dynamics. At the same time, built on FLIM, the pulses enter the fluorescence microscope, and the emission is detected on a single-photon basis by time-correlated single photon counting (TCSPC). The time-resolved detection allows species identification by their excitation lifetime. On the technical side, the TCSPC distinguishes the pumped and un-pumped signals on a shot-to-shot basis at MHz repetition rate (80 MHz in this work). PP-FLIM can be viewed as an application of F-PP in a confocal scanning microscope, with TCSPC detection. On the other hand, from the FLIM perspective PP-FLIM can be understood as a time-resolved extension of interferometrically resolved FLIM (ixFLIM) which we introduced recently.[39] ixFLIM is FLIM with

ACCEPTED MANUSCRIPT
The Journal of Chemical Physics
AIP Publishing
This is the author's peer reviewed, accepted manuscript. However, the online version of record will be different from this version once it has been copyedited and typeset.
PLEASE CITE THIS ARTICLE AS DOI: 10.1063/5.0319029

interferometric spectral resolution of the excitation spectrum, correlating the spectrum with emission lifetime. PP-FLIM then adds an additional dimension of the pump–probe delay.

We introduce the PP-FLIM technique, describe our proof-of-concept experimental setup, and demonstrate its capability on two types of samples. First, we measure a mixture of two fluorescent dyes, cresyl violet (CV) and oxonol VI (Oxo VI), in aqueous solution. Powered by the fluorescence lifetime resolution, PP-FLIM can disentangle the transient dynamics of the two noninteracting dyes with heavily overlapping spectra. The second experiment is a measurement of the PP dynamics within a single chloroplast in a spinach leaf (Spinacia oleracea L.), showcasing the imaging potential of PP-FLIM as well as its applicability to fragile biological samples.

II. PP-FLIM: F-PP with FLIM detection

A. Fluorescence-Detected Pump-Probe Spectroscopy

While PP-FLIM can be understood as a variant of FLIM with fast time resolution by PP, in this work we describe PP-FLIM as a variant of fluorescence-detected pump–probe spectroscopy detected by FLIM. The main concepts of fluorescence-detected PP (F-PP) spectroscopy have already been described in a few publications[25–27] therefore, only a brief outline of the core principles and a comparison of fluorescence PP and more traditional methods will be provided here.

In PP spectroscopy, the signals are traditionally classified as ground state bleach (GSB), stimulated emission (SE) and excited state absorption (ESA). In the conventional transient absorption, the GSB and SE lead to less signal photons (less absorption, additional stimulated emission), resulting in a negative signal. In contrast, the ESA increases the absorption, leading to a positive PP signal. Both the SE and ESA probe the excited state dynamics, the SE by a transition to ground state, ESA to higher excited states of the given sample. In a F-PP setup, the fluorescence induced by the probe beam is detected, isolating the difference with and without the preceding pump pulse. As the acquisition of data does not rely on the detection of a coherent signal, both collinear and non-collinear arrangement of the pump and probe beams is possible. For microscopy, the collinear configuration, as is the case presented here, is much easier to implement. The probe spectral resolution is in F-PP obtained interferometrically, using a pair of probe pulses, same as in the ixFLIM technique previously mentioned. Note, that the interferometric scan of the probe double-pulse does not compromise the pump–probe time resolution, since the time-ordered nonlinear response of to the pulses is measured.[25,40] In F-PP, same as in transient absorption, the GSB and SE signals are negative, since they result in less fluorescence induced by the probe. The reader is referred to ref.[25] for a full discussion on these processes in fluorescence PP measurements. In principle, the ESA would have a positive sign in the F-PP spectra, reflecting an increase in the detected fluorescence intensity. However, typically molecules rapidly relax non-radiatively from electronic states S_2 and higher, accessed by ESA. This results in an exceptionally low fluorescence quantum yield for this mechanism; thus, the ESA processes are effectively

ACCEPTED MANUSCRIPT
The Journal of Chemical Physics
AIP Publishing
This is the author's peer reviewed, accepted manuscript. However, the online version of record will be different from this version once it has been copyedited and typeset.
PLEASE CITE THIS ARTICLE AS DOI: 10.1063/5.0319029

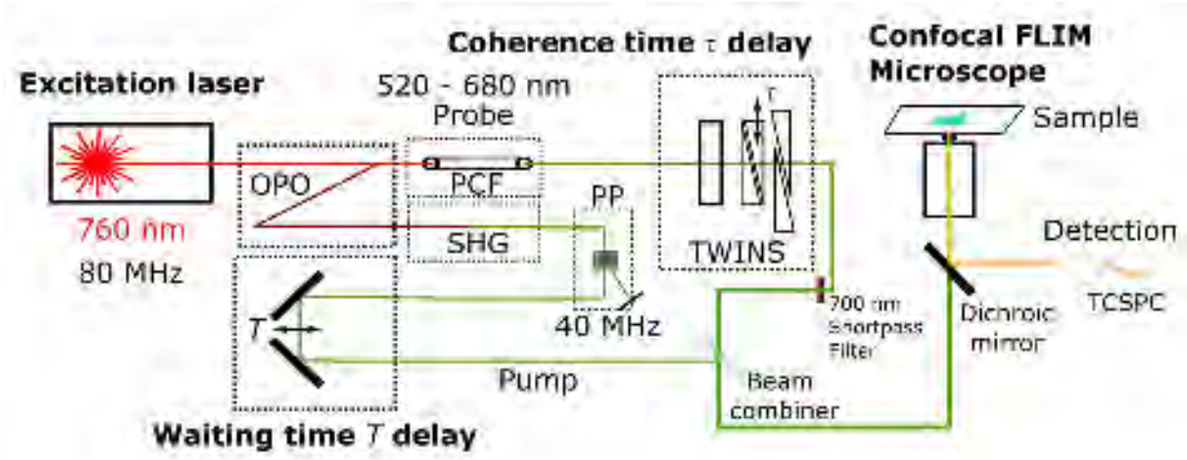

Figure 1 Optical setup of the pump-probe fluorescence lifetime imaging microscopy (PP-FLIM). The Ti:sapphire oscillator generates excitation pulses at 760 nm and a repetition rate of 80 MHz. OPO stands for optical parametric oscillator, PCF is a photonic crystal fiber producing a supercontinuum light with a wavelength range of 520 – 680 nm after passage through a 700 nm shortpass filter. SHG is second harmonic generation, and TCSPC stands for time-correlated single-photon counting. PP is a pulse picker which converts the repetition rate of the pump to 40 MHz. The pump–probe delay time T is controlled by a motorized stage with a retroreflector. The coherence delay time τ is scanned by wedge-based identical pulse encoding system (TWINS).[43,44]

invisible to fluorescence-detected PP setups. The excited-state dynamics is then determined from the SE signal. This simplification of the signal often provides a clearer picture than standard TA,[25,26] as exemplified in this article in the analysis of the Stokes shift dynamics of a dye mixture. PP-FLIM extends the F-PP on the detection side, resolving the fluorescence spatially, in this work by confocal microscopy, and temporally, here by time-correlated single-photon counting (TCPS). The spatial resolution provides the microscopy imaging, while the fluorescence time resolution allows separation of the pumped and un-pumped signals, as well as identification of the emitting species.[36,39]

B. PP-FLIM Experimental Setup

A schematic diagram of the PP-FLIM experimental setup can be seen in Figure 1. The fundamental laser light is generated by a Ti:sapphire oscillator (Coherent Chameleon Ultra II) which provides a train of ~150 fs, 40 nJ pulses at 760 nm. The repetition rate of these pulses is 80 MHz, which is high enough to allow for detection of high enough photon counts per second to acquire even weak fluorescence signals, and potentially obtain fast enough image scanning for experiments involving single molecules or micro-organisms.[41,42] This train of light is then passed to a spectrally tuneable optical parametric oscillator (OPO, Coherent Chameleon Compact OPO), generating pulses at 1160 nm for the dye mixture measurements or 1220 nm for the chloroplast experiment. To serve as the pump, the pulses are frequency doubled to 580 nm and 610 nm, respectively, by second harmonic generation (SHG, APE HarmoniXX SHG), and their repetition rate is halved to 40 MHz using a pulse picker (APE PulseSelect). The pump wavelength can also be modified thanks to the tunability of the signal output of the OPO. The remaining fundamental light not frequency converted by the OPO, with pulse energy about 4 nJ, is used for the supercontinuum generation in a custom-made photonic crystal fiber (PCF,

ACCEPTED MANUSCRIPT
The Journal of Chemical Physics
AIP Publishing
This is the author's peer reviewed, accepted manuscript. However, the online version of record will be different from this version once it has been copyedited and typeset.
PLEASE CITE THIS ARTICLE AS DOI: 10.1063/5.0319029

module SUP-2-125 by Photonics Bretagne), see section S1 in the Supplementary Material for details. After a 700 nm shortpass filter (Thorlabs FESH0700), we obtain probe pulses at 80 MHz covering 520 – 680 nm spectral range, as displayed in Figure 2a, b. More details on the ultrabroadband pulse generation can be found in our recent ixFLIM work.[39] A pulse pair is then formed using a birefringent common-path interferometer known as translating wedge-based identical pulse encoding system (TWINS),[43–45] to achieve controllable spectral modulation of the probe as described in the ixFLIM paper. The pump and probe beams are then collinearly combined using an ultrafast beam splitter (Thorlabs UFBS5050). The resulting 80 MHz excitation pulse train alternates between 'pumped' and 'unpumped', depending on the presence and absence, respectively, of the pump pulses. Control of the pump-probe delay time, T, is achieved by a delay line consisting of a motorized linear translation stage (Newport DL325) with a silver broadband retroreflector (Newport UBBR2.5-5S). The pump pulse energy was about 5 fJ at the sample position, the probe pulse energy with overlapped pulse-pair (τ=0) was adjusted to provide the same emission flux as the pump itself. The prepared beam was passed through a custom-made telescope to reduce the beam sizes by 50%, free space coupled into an inverted IX83 microscope with FV1200 confocal scanner (Olympus) and focused into the sample by an apochromatic UPLSAPO 60XW NA 1.2 water immersion objective (Olympus). This microscope offers a diffraction-limited spatial resolution up to around 0.2 µm at visible wavelengths.[46]

To fully reject the excitation light, the fluorescence emission from the sample is collected through a 700 nm longpass filter (Thorlabs FELH0700) and guided via multimode optical fiber to a cooled GaAsP hybrid photomultiplier tube (PicoQuant, PMA Hybrid 40). Signal is processed by a TimeHarp 260-PICO TCSPC card and a custom script written on a snAPI python wrapper triggered by the scanner (both PicoQuant). The frame acquisition is triggered by a custom-made script in Matlab (Mathworks) providing full control of all components outside the microscope. Reference spectra of the pump and probe beams at the entrance of the microscope are collected by a fibre spectrometer (Ocean Insight SR-2).

As with any pump-probe experiment, it is important to determine the time zero, i.e. the relative time-delay where the pump and probe pulses temporally overlap, $T = 0\ s$. In F-PP, and thus PP-FLIM, this is complicated by the presence of negative-time-delay signal with GSB spectral shape.[25,26] As a fast nonlinear process localized at time zero, two-photon excitation of the laser dye coumarin 450 was used to determine this point. For this purpose, coumarin 450 was recrystallized from ethanol onto a microscope slide and excited with the 610 nm pump pulse, while the probe was spectrally restricted to a 50 nm narrow band around 600 nm using a bandpass filter (Chroma). The delay line T was then scanned, and the resulting blue two-photon fluorescence was detected through a 435/40 nm bandpass filter (Semrock). Since coumarin 450 absorbs in UV, the emission must result from the two-photon excitation induced by the temporal overlap of the pump and probe pulses. The time-zero ($T = 0$) was determined from the maximum fluorescence intensity observed during the translation of the delay stage. A plot of the two-photon fluorescence intensity as a function of the pump-probe

ACCEPTED MANUSCRIPT
The Journal of Chemical Physics
AIP Publishing
This is the author's peer reviewed, accepted manuscript. However, the online version of record will be different from this version once it has been copyedited and typeset.
PLEASE CITE THIS ARTICLE AS DOI: 10.1063/5.0319029

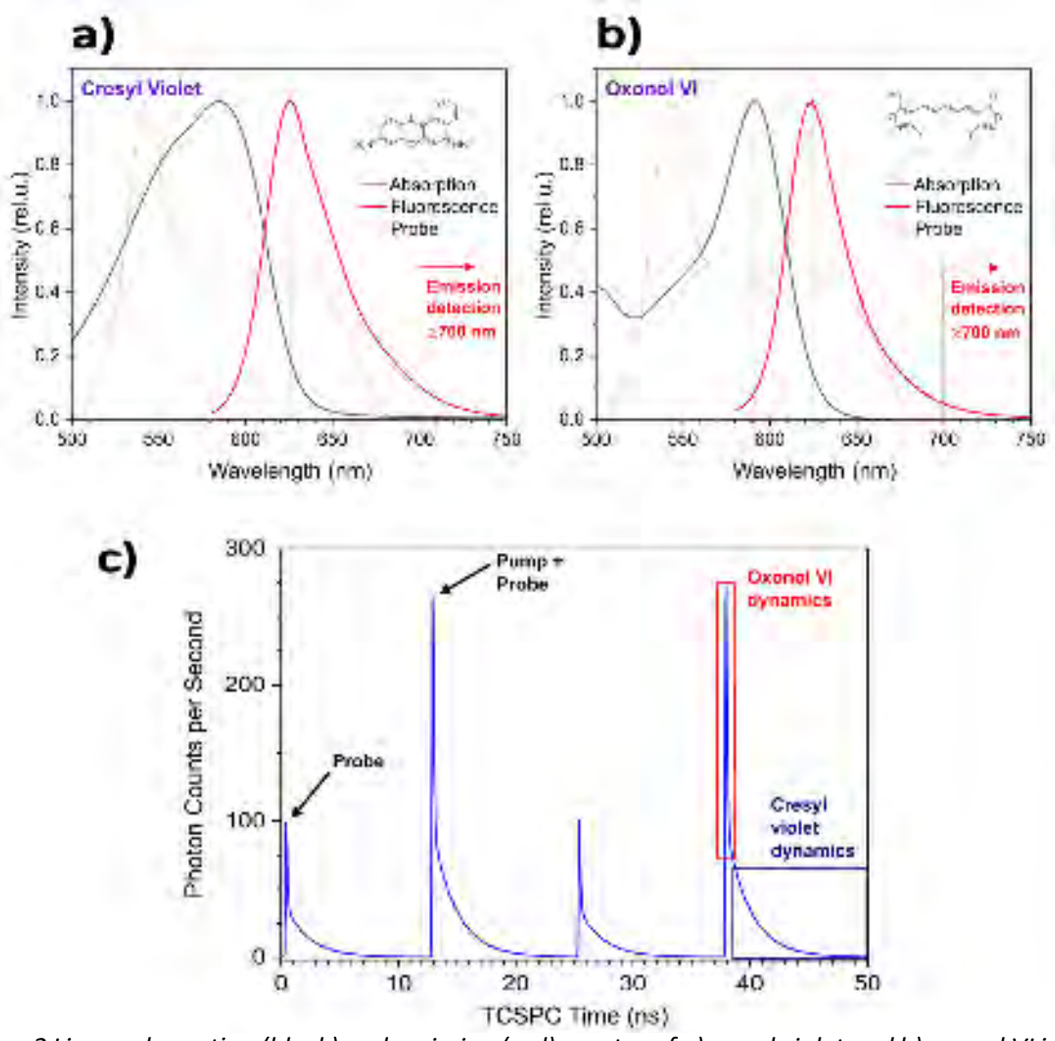

Figure 2 Linear absorption (black) and emission (red) spectra of a) cresyl violet and b) oxonol VI in water. Probe spectrum is shown in orange, the detection region is indicated. Insets show the chemical structure of the dyes. c) Exemplary TCSPC histogram from the dye mixture, showing the alternating probe-only and pump and probe-induced fluorescence decays. Indicated are also the time gate regions for oxonol VI (red) and cresyl violet (blue).

delay is shown in Fig. S2 of the Supplementary Material.

Due to the broad spectral range of the probe and its complex optical path including the propagation in the PC, there is a pulse chirp at the focal point, that we did not compensate. To determine this chirp, a fraction of the supercontinuum (624 – 680 nm) was focused onto a BBO crystal placed at the sample position, and the intensity of the sum-frequency generation of the pump and probe beams was detected for each probe wavelength by a fibre spectrometer (Ocean Insight SR-2). The pump–probe delay was scanned, allowing to determine the sum-frequency intensity as a function of wavelength, λ and delay time, T. Gaussian curves were then fitted to the temporal profiles at individual wavelengths, which provided wavelength-dependent time-zero points at the curve centres. To fit the temporal supercontinuum chirp, we take into account the pulse group-delay dispersion (GDD) and third-order dispersion (TOD). Thus, upon converting the wavelengths to angular optical frequency, a parabolic fit was employed as a function of this frequency (see Eq. S1 in the Supplementary Material), which

ACCEPTED MANUSCRIPT
The Journal of Chemical Physics
AIP Publishing
This is the author's peer reviewed, accepted manuscript. However, the online version of record will be different from this version once it has been copyedited and typeset.
PLEASE CITE THIS ARTICLE AS DOI: 10.1063/5.0319029

provides a chirp correction based on both GDD and TOD. The results of this fit were then used to correct the time zero as a function of wavelength in the pump-probe data in the whole probe spectrum wavelength range. Details of the chirp determination and subsequent data correction can be found in Section S3 of the Supplementary Material.

C. Data Acquisition and Processing

We demonstrate the data acquisition and processing on a PP-FLIM measurement of an aqueous mixture of 2.7 mM cresyl violet perchlorate (CV, Exciton) and 8.1 mM oxonol VI (Oxo VI, Exciton), both used as received. The Oxo VI concentration was chosen to obtain a comparable emission signal from both dyes. The chemical structures of CV and Oxo VI are shown in Fig. 2a and Fig. 2b, respectively. The linear absorption and fluorescence spectra of both dyes are shown in Fig. 2a and b as well, together with the probe spectrum. The longpass filter was used to select red-tail emission for detection, as indicated. For the pump-probe experiments, 60.0 µL of the dye solutions were mixed and dropped onto a microscope dish. The microscope was focused 30 µm deep into the sample to suppress surface-related dynamics. Pump-probe data was measured at 20 T delays ranging from -500 to 1200 ps. For each T, 301 τ delays of the TWINS centred around $\tau = 0\ s$ were recorded with the step of 0.75 fs. To obtain the final pump-probe data, the measurements was averaged over 16 T scans for each sample.

The processing of the data was performed by a modified version of the Matlab script used in the previous ixFLIM measurements.[39] Since the mixture is spatially uniform, the spatial scanning serves in this case for averaging, replacing the need to flow or move the sample. A total, spatially integrated photon-count histogram of the fluorescence decay of the sample measured by the TCSPC was thus exported for each T and τ step. An example of such a TCSPC histogram is shown in Fig. 2c, with a channel width of 50 ps and total time-window of 50 ns. One can clearly distinguish decays induced by four consecutive excitation pulses, pulse one and three is the probe only, pulses two and four comprise both the pump and probe. The decays reflect the short lifetime of Oxo VI, and the longer-lived CV emission.

The interference-modulated excitation laser spectra were measured for each τ and *T* delay as well. The comparison of the spectrometer-measured wavelength λ with the interferometric λ_τ obtained by the Fourier transform, described below, was used for calibration. The Fourier transform removes the pump contribution, and the resulting spectrum can be used as a reference. The sample excitation and pumped spectra were obtained by a Fourier transform along τ, following the procedure described in the publication on the ixFLIM experiment,[39] using the un-pumped and pumped traces in the TCSPC histograms, respectively. The Fourier transform removes the pump-only-induced fluorescence, as this does not depend on τ. To suppress noise, the TCSPC traces were windowed for the Fourier transform using a Hann function $w(\tau) = \sin^2\left(\frac{\pi\tau}{\tau_{range}}\right)$, where $\tau_{range} = 60$ fs. The resulting windowed spectra were divided by the reference probe spectrum to obtain the transient spectra of the sample

ACCEPTED MANUSCRIPT
The Journal of Chemical Physics
AIP Publishing
This is the author's peer reviewed, accepted manuscript. However, the online version of record will be different from this version once it has been copyedited and typeset.
PLEASE CITE THIS ARTICLE AS DOI: 10.1063/5.0319029

independent of the spectrum or intensity fluctuations of the probe beam. The advantage of this approach is that the excitation spectrum and pump–probe spectrum are acquired quasi-simultaneously. The excitation spectrum can thus be used to correct for potential sample bleaching and to check the sample integrity in general.

So far, we have used the TCSPC time resolution simply to separate the pumped and un-pumped signals, integrating over the whole TCSPC decay histograms from the respective pulses. The TCSPC, however, also contains information about the emitting species, which can be used to disentangle their F-PP spectra. In case of our dye pair, this can be done by straightforward signal gating, due to their order-of-magnitude difference in lifetimes: ~80 ps for Oxo VI[47] and ~2 ns for CV.[48] To isolate the Oxo VI dynamics, a time gate can be set to acquire data up to 200 ps after excitation. In this way, most of the Oxo VI signal (>90%) is gated in and more than 90% of the CV signal is rejected. Similarly, the traces beyond 200 ps give information about the CV dynamics exclusively. With the PP data sets for the two dyes acquired and separated, the ultrafast (sub 50 ps) dynamics of these compounds can then be investigated.

The transient F-PP data were corrected for the probe chirp, with the pump-probe delay times adjusted at each wavelength according to the chirp, with 620 nm selected as the time-zero point. The PP data were then interpolated to these corrected times so that the rise of the PP signal began at the same time across the wavelength range. Thus, the rise time of the integrated transients across the GSB wavelengths for this dataset provides the cross correlation of the PP-FLIM instrument. This was fitted with an exponential function and was determined from the Oxo VI PP data to be 660 ± 100 fs. Further details on this process are available in Section S3 of the Supplementary Material.

For determining the time constants associated with the dynamics taking place within the PP data, a fitting function was used with an exponential component for each process and a convolution with the cross correlation of the PP-FLIM instrument, according to the convolution of an exponential decay with instrument response function (IRF) equation derived by van Stokkum *et al.*[49] If we let $\Delta = cc\sqrt{\log(2)}/2$, where cc is the measured cross correlation of the instrument, the dynamics involving decay or rise in population can be fitted with Equations (1) and (2) respectively:

$$I(T) = \frac{1}{2}A\exp\left(\frac{-T}{t}\right)\exp\left(\frac{1}{t}\frac{\mu+{\Delta^2}/{t}}{2}\right)\left\{1+\operatorname{erf}\left(\frac{T-\left(\mu+{\Delta^2}/{t}\right)}{{\sqrt{2}}/{\Delta}}\right)\right\} \quad (1)$$

$$I(T) = \frac{1}{2}A\exp\left(\frac{T}{t}\right)\exp\left(\frac{-1}{t}\frac{\mu+{\Delta^2}/{t}}{2}\right)\left\{1+\operatorname{erf}\left(\frac{-T+\left(\mu+{\Delta^2}/{t}\right)}{{\sqrt{2}}/{\Delta}}\right)\right\} \quad (2)$$

where $I(T)$ is the intensity of the signal as a function of T; t is the time constant for a dynamics process; A is the amplitude of the fitting function for a particular process; μ is the centre (in fs) of the IRF Gaussian curve; and erf refers to an error function. When fitting the transients of the PP data, an overall function summing the individual $I(T)$ functions for each of the dynamics occurring in the sample is used, with one additional contribution based on Equation

2 with a long lifetime to reflect the presence of longer-lived GSB.

III. RESULTS AND DISCUSSION

A. Fluorescent Dye Mixture

First, we discuss the PP-FLIM measurement of a laser dye mixture. This test is similar to the one performed by Tahara and coworkers to benchmark their two-dimensional fluorescence lifetime correlation spectroscopy setup.[50] The linear volume absorption and emission spectra of the two dyes, CV and Oxo VI, are given in Fig. 2a (CV) and Fig. 2b (Oxo VI). As mentioned above, the maximum absorption wavelengths obtained for CV and Oxo VI are very similar to each other, 585 and 590 nm respectively, in agreement with the literature.[39,51,52] The PP-FLIM experiment is also capable of providing an excitation spectrum of these dyes from the unpumped signals, a plot of these can be found in Fig. S7 in the Supplementary Material. This absorption band corresponds to the excitation to the first singlet excited state, S_1, in both dyes.[53,54] Similarly, the two dyes have a matching maximum emission wavelength of 625 nm measured here, from excitation at 580 nm to match the pump wavelength in the fluorescence PP experiment. The absorption spectrum of CV features a shoulder at the blue side of the absorption peak (around 550 nm), previously attributed to H-aggregates formed in in aqueous CV dye solutions.[55–57] CV has been known to readily form H-aggregates even in very dilute aqueous solutions, likely due to the chain of aromatic rings in the molecular structure forming π-stacking interactions.[57]

From the TCSPC histograms in the ixFLIM components of the PP-FLIM data, displayed in Fig. 2c, a bi-exponential decay function can be fitted to the un-pumped trace to determine Oxo VI and CV emission lifetimes. The recovered shorter lifetime of 109 ± 2 ps corresponds to Oxo VI (though the TCSPC time-bin is 50 ps), which is slightly slower than the 80 ps reported in the literature.[47] The longer CV-related lifetime was 2.19 ± 0.05 ns, which is comparable to the 2 ns reported for aqueous CV solutions.[48]

Moving our attention now to what the PP component of the PP-FLIM instrument provides, a map of the raw PP spectra of the dye mixture is presented in Figure 3a. The data show a clear red-shift after the zero-time delay, reflecting the dynamics of the Stokes shift visible in the SE signal. In these data, however, the overlapping dynamics of both dyes are present, with similar spectra and comparable time scales. Without any difference in their fluorescence lifetimes, it would be impossible to separate them. We can take advantage of this difference to extract the excitation, emission, and pump-probe spectra of the dyes individually (see Figure 2c). The resulting PP data separated between the Oxo VI and CV dyes are presented in Figures 3b and 3c, respectively. From the plots in Figure 3, we can see that at times $T < 0$, there is a band of negative intensities centred around 590 nm corresponding to the S_1 excitation of individual dyes, which reflect the GSB of the sample. This band is enhanced close to the time-zero by SE

ACCEPTED MANUSCRIPT
The Journal of Chemical Physics
AIP Publishing
This is the author's peer reviewed, accepted manuscript. However, the online version of record will be different from this version once it has been copyedited and typeset.
PLEASE CITE THIS ARTICLE AS DOI: 10.1063/5.0319029

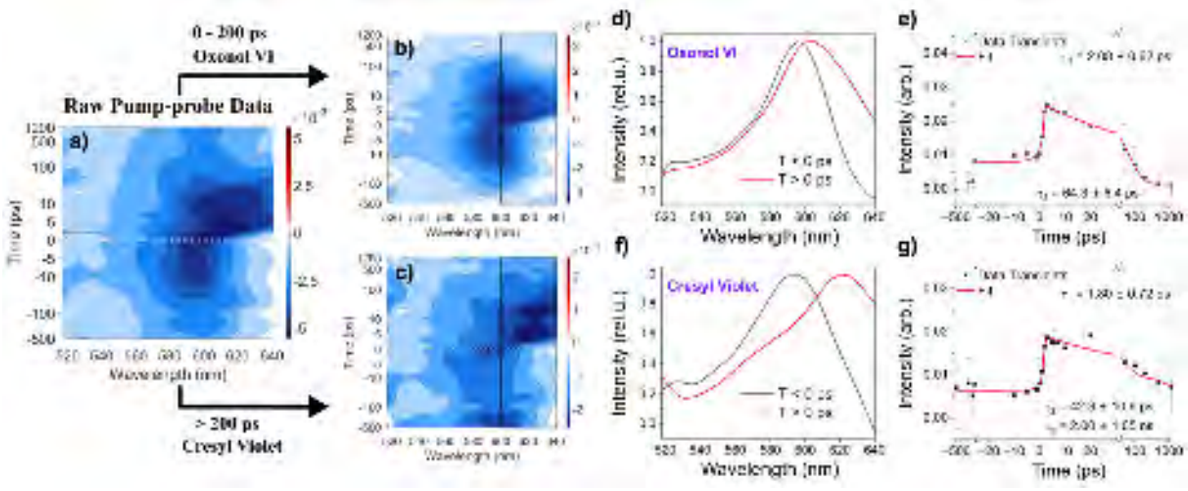

Figure 3 Raw fluorescence-detected PP map of the CV and Oxo VI mixture (a), separated by the time gating into that of Oxo VI (b) and CV (c) (see the main text for details). From the Oxo VI data, the time-integrated spectra at T < 0 and T > 0, respectively, are displayed in (d) to show the spectrum before and after the Stokes shift of the molecule. The transients between 600 – 640 nm (marked on panel b), along with the time constants from fitting, are displayed in (e). The same for the CV data is displayed in (f) and (g) respectively.

induced by the pump pulse incoming after excitation of the sample by the probe (note that the SE is thus not spectrally resolved). This SE band extends further into the negative pump-probe delays in the CV plot than it does in the Oxo VI plot, which directly relates to the difference in fluorescence lifetimes of these molecules. Another negative intensity band, centred at around 625 nm, appears straight after time-zero, which corresponds to the SE of the dyes from the S_1 state back to S_0. Again, this band has a longer decay time in CV than in Oxo VI that can be readily seen by eye. This is expected based on the fluorescence decay dynamics. Both dyes undergo an ultrafast excited-state Stokes shift,[17] easily seen around time zero from the rapid change of the centre wavelength of the minimum. The 'mean' centre wavelengths of the Stokes shift for each dye can be roughly determined by plotting the fluorescence PP signal as a function of wavelength integrated across T, separately for $T < 0$ ps and $T > 0$ ps, though care is required at times where the Stokes shift is biased by the continued presence of GSB at positive T times, together with SE.[26] The time scale of the Stokes shift can also be determined from the F-PP transients by integrating the spectra between 600 and 640 nm (to cover the aftermath signals from the Stokes shift) for each T step after time zero.

For Oxo VI, the transient spectra before and after the Stokes shift are shown in Figure 3d, where the wavelength of the lowest PP signal shifts from 590 nm to 605 nm. The transients of Oxo VI in the range of 600 – 640 nm are plotted in Figure 3e. The fit to the model described earlier is also presented as a red line, along with the resulting fit parameters. The Stokes shift was found to occur with a time constant of 2.08 ± 0.62 ps, which corresponds to the timescale of Stokes shifts previously observed for fluorophores in aqueous solutions.[58,59] The time constant for the excited-state decay is 64.3 ± 6.4 ps, which is somewhat faster than the time constant found from the raw TCSPC trace of this dye molecule. A difference between the

ACCEPTED MANUSCRIPT
The Journal of Chemical Physics
AIP Publishing
This is the author's peer reviewed, accepted manuscript. However, the online version of record will be different from this version once it has been copyedited and typeset.
PLEASE CITE THIS ARTICLE AS DOI: 10.1063/5.0319029

ACCEPTED MANUSCRIPT
The Journal of Chemical Physics
AIP Publishing
This is the author's peer reviewed, accepted manuscript. However, the online version of record will be different from this version once it has been copyedited and typeset.
PLEASE CITE THIS ARTICLE AS DOI: 10.1063/5.0319029

excited-state lifetime obtained by the FLIM and the F-PP parts of PP-FLIM can be expected because of additional anisotropy kinetics. While the fluorescence was not polarization resolved, the parallel pump and probe polarizations lead to an additional anisotropy decay of the F-PP transients. Since the rotational time of small dyes such as oxonol is typically several hundreds of picoseconds,[60] the additional anisotropy decay shortens the F-PP decay time.

Similar data are shown in Fig. 4f and Fig. 4g for CV. In this case, the peak shifts from 590 to 620 nm, in perfect agreement with the spectral characteristics of this molecule. The transients in the 600 – 640 nm wavelength band are plotted in Fig. 3g. For CV, the Stokes shift was found to have a time constant for the rise in signal at this wavelength range of 1.80 ± 0.72 ps, similar in timescale to that of Oxo VI (both results are within the error margins of each other). The SE decay time constant was also determined at 2.00 ± 1.05 ns, which is in fairly good agreement with the literature and similar to the results from the TCSPC traces, albeit with a larger error due to a relatively low signal-to-noise ratio compared to Oxo VI. This lower signal-to-noise ratio results from a much smaller number of counts in the relevant TCSPC bins for this dye. Curiously, unlike in the Oxo VI transient data, a model with two time constants was not able to produce a satisfactory fit, and a third decay component had to be incorporated, with a time constant of 42.3 ± 10.6 ps. Since the reported rotational anisotropy decay time of CV is longer,[61] we attribute the component mainly to an intersystem crossing to a triplet state, previously reported for relatively poorly fluorescent H-aggregates of CV on a SiO_2 surface with time constant of 35 ps.[62] This provides another example of excited-state dynamics that cannot be directly observed by conventional FLIM, due to its limited temporal resolution and spectrally unresolved signal.

Overall, the new PP-FLIM method demonstrates the ability to separate and characterise ultrafast excited-state dynamics of dye molecules in a mixture through fluorescence-detected PP component, which conventional FLIM or ixFLIM cannot access. This capability is chiefly demonstrated by the determination of the individual extent and dynamics of the Stokes shift of two dyes in the mixture. We stress that, thanks to the microscopy-based approach, this measurement was performed using less than 100 µL of sample, and spatial scanning replaced the sample movement or flow commonly used in standard ultrafast experiments.

B. Chloroplast in Spinach Leaf

In order to demonstrate the imaging capability of the PP-FLIM instrument, along with its ability to characterize fragile biological samples that are prone to bleaching, we measured single chloroplasts in a spinach leaf (*Spinacia oleracea L.)*. The chloroplasts contain densely-packed thylakoid membrane, at which reside the photosynthetic photosystems I and II.[63] The expected photo-induced dynamics comprise photosystem excitation followed by energy transfer to the reaction centre.[14] Two FLIM images are displayed in Fig. 4a. These PP-FLIM images are in excellent agreement with published FLIM data of chloroplast in leaves by Wientjes et al., regarding the fluorescence lifetimes of photosystems I and II, as well as the chloroplast inner structure showing the thylakoid grana (blurred by the diffraction limit).[64,65]

ACCEPTED MANUSCRIPT
The Journal of Chemical Physics
AIP Publishing
This is the author's peer reviewed, accepted manuscript. However, the online version of record will be different from this version once it has been copyedited and typeset.
PLEASE CITE THIS ARTICLE AS DOI: 10.1063/5.0319029

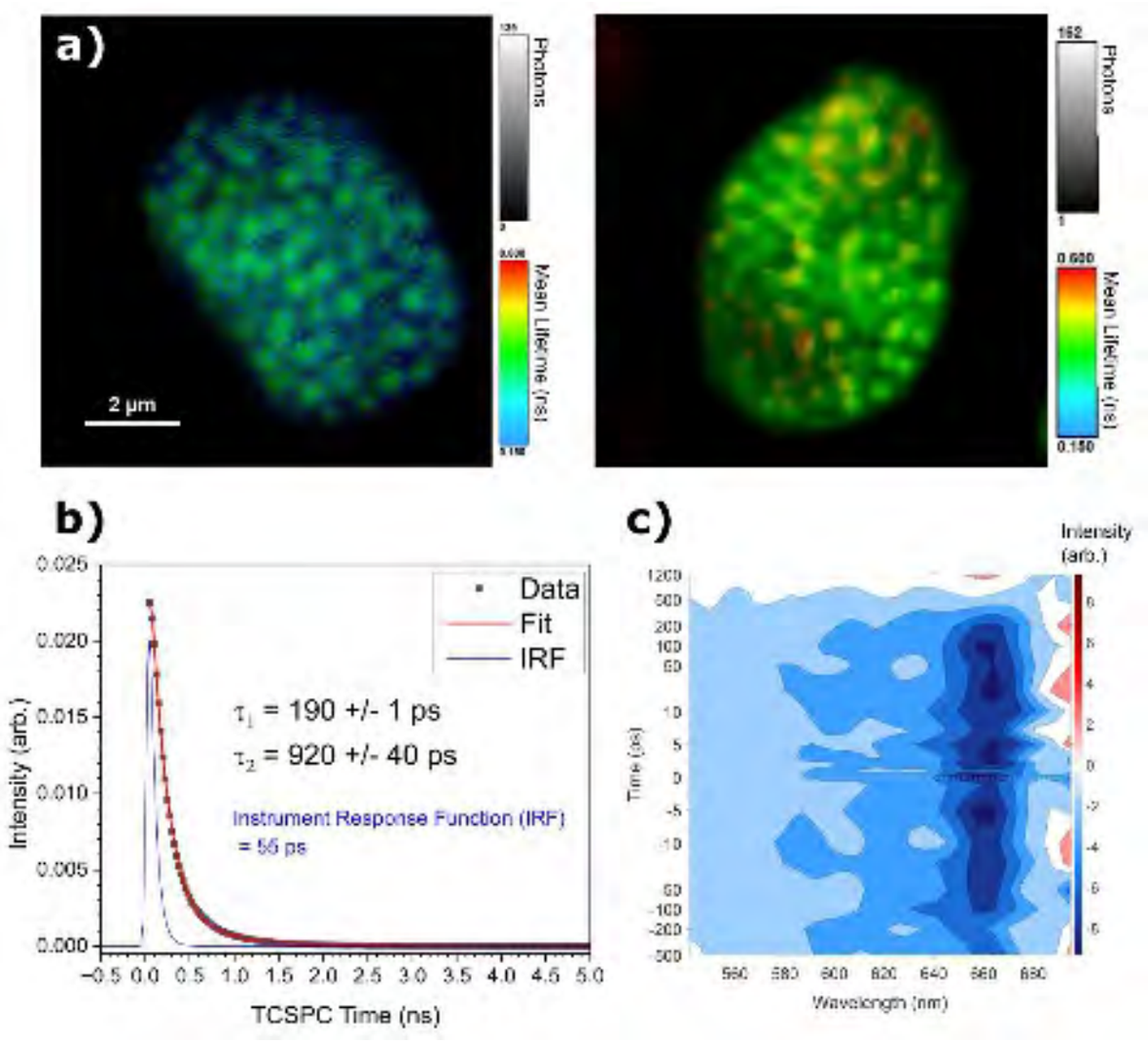

Figure 4 PP-FLIM of intact chloroplasts. (a) FLIM images of two chloroplasts in an intact leaf of spinach (a). (b) The fluorescence decay trace averaged over four chloroplasts, with a bi-exponential fit. The instrument response function of the TCSPC was taken into account in this fit, 55 ps. (c) The mean pump-probe transient spectrum taken from cumulative data of four chloroplasts.

The TCSPC traces averaged over four PP-FLIM measurements of single chloroplasts are given in Fig. 4b, along with a bi-exponential fit applied to the data sets to obtain two fluorescence decay time constants. This fitting model also took into consideration the instrument response function (IRF) of the TCSPC system, with an IRF value of 55 ps used as the cross-correlation (*cc*) in Eq. (1), where the two exponential decay functions were implemented. From the TCSPC traces shown in Fig. 4b, two time constants were extracted. The fast component was determined to be 190 ± 1 ps, and the slower component was 920 ± 40 ps. Xu et al. performed a series of ultrafast spectroscopic studies on chloroplasts in leaves of several plants, including spinach, and extracted three time constants.[66] Their fast and slow components, 190 and 1378 ps respectively, show reasonably good agreement with our measured time constants, particularly for the fast component.

Fig. 4c shows the mean transient pump–probe excitation and stimulated emission spectrum

ACCEPTED MANUSCRIPT
The Journal of Chemical Physics
AIP Publishing
This is the author's peer reviewed, accepted manuscript. However, the online version of record will be different from this version once it has been copyedited and typeset.
PLEASE CITE THIS ARTICLE AS DOI: 10.1063/5.0319029

acquired from our four measurements. The transient signal persists from approximately -200 ps to +200 ps, in rough agreement with the dominant 213 ps decay time obtained from the TCSPC histogram, corresponding to the excitation lifetime of the photosystems within the chloroplast.[65,67] The transient kinetics are, however, not exponential but are rather flat. A possible explanation could involve processes such as singlet–triplet annihilation, expected at such a high pulse repetition rate, where the inter-pulse delay is shorter than the triplet lifetime. The lack of any time constant on the order of nanoseconds suggests that the signal does not arise from free chlorophyll molecules or photo-damaged complexes.[68] While there is possibly a red shift observed at positive delay times, this effect is rather small. This is expected due to the large number of chlorophylls in the photosystems and the resulting incoherent mixing of linear signals via exciton–exciton annihilation, as described in the following section.[69]

There is also a peculiarity in the data to note: while the lifetimes from the TCSPC traces match those of the photosystems, the absorption band around 660 nm does not, since the photosystems are expected to absorb at around 680 nm.[64,65] Our best explanation for this is is the presence of an inner spectral filter effect, where the high optical density (OD) of the chloroplast-packed leaf as a whole is causing increased absorption at the red end of the probe spectrum before it reaches the focus at the chloroplast being measured deeper within the sample.[70] The red edge of the probe is thus strongly attenuated, suppressing the SE contribution to the spectra, and, consequently, the excited-state dynamics as well. This includes both excited-state relaxation and the possible Stokes shift. Since these measurements were proof-of-principle, further analysis and possibly further experiments aimed at clearer excited-state dynamics, e.g., by the suppression of the incoherent mixing, would be required before drawing any definitive conclusions about the photosystem photo-induced dynamics.

In general, the demonstrated ability to image single chloroplasts within an intact leaf, as seen in Fig. 4a, along with the acquisition of the PP spectra clearly highlights the imaging potential of the method to probe local environments within a large system. This opens a wide variety of possible studies to gain further insight into chemical and biological processes where only a general dynamics mechanism of the ensemble of the system have been characterized so far, such as in photosynthetic systems or other photoactive materials.

C. Discussion: properties of PP-FLIM

Despite the demonstrated successes of the PP-FLIM approach discussed in this article, there are several limitations that must be carefully considered when employing this technique. Generally, action-detected spectroscopic techniques such as this one may encounter situations in which the detected signal is not proportional to the number of excitons generated upon excitation of the sample. Such nonlinear effects include exciton-exciton annihilation, where an encounter of two excitons leads to a net loss of one exciton, quenching the fluorescent signal detected.[71] Such loss incoherently mixes the linear response from otherwise independent excitations, effectively masking the nonlinear response of the system excited state.[69,72,73] As a consequence, the excited-state dynamics associated with the stimulated emission (SE)

ACCEPTED MANUSCRIPT
The Journal of Chemical Physics
AIP Publishing
This is the author's peer reviewed, accepted manuscript. However, the online version of record will be different from this version once it has been copyedited and typeset.
PLEASE CITE THIS ARTICLE AS DOI: 10.1063/5.0319029

component of the signal can be obscured by a large stationary mixing background, as observed in the measurements on spinach leaves presented here. Possible strategies to mitigate incoherent mixing have been proposed, such as subtracting the negative-delay (T<0) signal from the positive-delay (T>0) transient signal, which removes stationary background contributions, including incoherent mixing.[74] In practice, however, the extent to which such mixing can be removed is limited by the signal-to-noise ratio and by the effective size of the system under study. Since the negative-time data reflect the ground-state spectrum, contrasting it with the T>0 dataset can in general help to discern the excited-state dynamics such as dynamic Stokes shift.[26] The ground-state-related negative-time PP-FLIM signal cannot be in general removed directly in the data acquisition. However, as seen from Fig. 3a-c, the negative-time signal is absent at the red edge, in which only stimulated emission contributes (SE). This observation provides a hint to an experimental arrangement eliminating the T<0 signal. Using a probe beam of red-shifted spectrum, such that it by itself does not excite the sample, reduces the F-PP data to the SE signal only, vanishing for T<0 and reporting on the excited-state dynamics for T>0[25,26].

The fluorescence lifetime dimension allows one to disentangle the emitting species, as demonstrated on the oxonol/cresyl violet mixture. While this was to a degree an artificial system, such decomposition can be used anywhere where FLIM identifies multiple decay species. Standard analysis methods such as global analysis[49] or maximum entropy analysis[50] can be used, and each decay component will have a transient pump–probe spectrum associated with it. Note, that additional resolution of the emitted fluorescence spectrum is possible in PP-FLIM, for example by the means of another TWINS interferometer in the detection arm[75], or with the recently available SPAD arrays.

In its current implementation, the data acquisition speed of the PP-FLIM is considerably slower than that of conventional pump-probe methods with direct spectral resolution. This limitation arises from the need to scan the coherence time τ in order to obtain spectral information via Fourier transformation. As discussed previously in the article introducing the ixFLIM technique, an ixFLIM measurement typically requires several minutes, depending on parameters such as the microscope scanning speed and the number of pixels in the image.[39] Within the PP-FLIM configuration, this acquisition time corresponds to the pump-probe data at a single pump-probe delay. Consequently, acquiring high-resolution images at multiple delay times – 20 delays in the measurements presented here – results in a total measurement time of approximately one hour. This presents a significant limitation for samples that are prone to photobleaching, which must be mitigated by reducing the number of pixels acquired. Conversely, for samples in which high spatial resolution is not critical, such as the dye measurements discussed here, acquisition times can be substantially reduced by decreasing both the number of scanned pixels and the dwell time per pixel. Another possible way to reduce the acquisition time is more efficient sampling of the time delays, such as undersampling or compressed sampling of the probe pulse pair interferogram.[76,77]

ACCEPTED MANUSCRIPT
The Journal of Chemical Physics
AIP Publishing
This is the author's peer reviewed, accepted manuscript. However, the online version of record will be different from this version once it has been copyedited and typeset.
PLEASE CITE THIS ARTICLE AS DOI: 10.1063/5.0319029

PP-FLIM has, however, an inherent advantage over standard transient absorption regarding photobleaching due to the resonance fluorescence detection. While the photo-induced sample damage can occur even at the low pulse energies used, and did occur for example in our chloroplast measurement (typically about 25% bleaching over the course of the whole 30-minute PP-FLIM scan), the bleached sample typically does not fluoresce, at least not with the same lifetime and in the same spectral region. Furthermore, with PP-FLIM the fluorescence excitation (ixFLIM) is acquired simultaneously as the un-pumped reference. The excitation spectrum can thus be used to check the integrity of the sample, and possibly normalize the signal on the total fluorescence counts.

For the PP-FLIM instrument described here, the primary limitation in improving the signal-to-noise ratio arises from the generation of the probe supercontinuum. Although the relatively high repetition rate of the laser system (80 MHz) is advantageous for accumulating signal efficiently over the measurement time, and the correspondingly low pulse energies are well suited for samples sensitive to photobleaching, this combination poses challenges for stable white-light generation. In the present setup, the supercontinuum generated with the photonics crystal fibre (PCF) over the 520 – 680 nm range exhibited an average intensity noise of approximately 2% across the spectral bandwidth. When compared with the nonlinear signal level, which reached a maximum about 10% of the total detected intensity in the dye measurements, this noise level necessitated multiple repeated acquisitions to achieve an acceptable signal-to-noise ratio. The performance of the instrument could therefore be improved by incorporating a laser system with tuneable repetition rate and output power, optimized for each individual sample.

With regard to spatial resolution, the current setup uses conventional confocal microscopy, for which the resolution is fundamentally limited by the optical diffraction. Under typical conditions, this results in a best achievable lateral (x-y) resolution of approximately 200 nm, and an axial (z) resolution of around 500 nm. The actual resolution further depends on the pump and probe wavelengths as well as on the numerical aperture of the microscope objective.[78] It is worth mentioning, though, that the spatial resolution is ultimately given by the nonlinear PP signal generation in the overlap of the pump and probe beams. This means that, for the same pump and probe spot sizes, the point spread function (PSF) is narrower than that given by linear fluorescence imaging.[79] Moreover, the use of pump-probe combination opens the possibility of achieving even higher spatial resolution through PSF shaping, possibly approaching a quadratic diffraction limit.

A summary of the key characteristics of the PP-FLIM instrument is provided in Table 1, along with a comparison to conventional FLIM and transient absorption spectroscopy techniques.

Table 1 Comparison of key properties of FLIM, TA, and PP-FLIM

	FLIM	**TA**	**PP-FLIM**
Spatial resolution	3D, linear diffraction limit (~200 nm)	2D, spot size (~100 um)	3D, Quadratic diffraction limit

ACCEPTED MANUSCRIPT
The Journal of Chemical Physics
AIP Publishing
This is the author's peer reviewed, accepted manuscript. However, the online version of record will be different from this version once it has been copyedited and typeset.
PLEASE CITE THIS ARTICLE AS DOI: 10.1063/5.0319029

			(~150 nm)
Time resolution	Photon counting by TCSPC (~50 ps)	Ultrafast, defined by pulses (~15 fs)	Ultrafast, defined by pulses* (~20 fs)
Sensitivity	Down to single molecules[80]	Between one part in ten thousand to a million[81,82]	Down to single molecules potentially[27]
Types of signal	Spontaneous emission	GSB, SE, ESA	GSB,SE
Data acquisition Time	Few minutes with TCSPC[35]	Typically, at least 15 minutes for a full scan (~100 T steps)[83]	Around 30 minutes for 20 T steps per scan.
*trade-off between temporal and spatial resolution, dependent on microscope objective			

The present work constitutes a proof-of-principle experiment and is currently limited in both time resolution and signal-to-noise ratio by the oscillator laser source, necessitating the use of a photonic crystal fibre (PCF) for white light generation. However, laser systems currently available provide sufficient pulse energy at MHz repetition rates to generate shorter and more stable broadband pulses.[84] Adaptation of the present PP-FLIM setup in this direction is presently underway.

IV. CONCLUSIONS AND OUTLOOK

To summarize, PP-FLIM is a combination of fluorescence-detected pump–probe (F-PP) transient absorption and fluorescence lifetime imaging microscopy (FLIM). FLIM detection, in addition to enabling shot-to-shot acquisition at high repetition rates, allows measurement of small sample volumes as well as spatial imaging of fragile samples with three-dimensional optical resolution while identifying the emitting species by their fluorescence lifetime. The PP excitation pulse sequence then adds ultrafast time resolution of the excitation dynamics, from absorption to emission. As reviewed in Table 1, the PP-FLIM thus benefits from the single-photon counting sensitivity of TCSPC FLIM imaging as well as the time resolution of pump–probe spectroscopy. Samples well suited for PP-FLIM are those with relatively small effective system size and pronounced stimulated emission dynamics.

We have demonstrated the performance of PP-FLIM through measurements of an aqueous mixture of two fluorescent dyes, CV and Oxo VI. By exploiting the difference in fluorescence lifetimes of the two molecules, the individual TA dynamics were successfully isolated for each dye. In addition to the good agreement in the decay time constants observed in the stimulated emission (SE) of each dye between the TCSPC-detected transients and the PP transients, the PP component of the instrument also successfully probed the ultrafast Stokes shift dynamics of the dyes following photoexcitation. Furthermore, the imaging and measurement of the PP dynamics of a single chloroplast within an intact spinach leaf, at femtojoule pulse energies, demonstrate the imaging capability of PP-FLIM, even for biological samples.

We envisage two main areas of PP-FLIM application, dependent whether one sees it as an

ACCEPTED MANUSCRIPT
The Journal of Chemical Physics
AIP Publishing
This is the author's peer reviewed, accepted manuscript. However, the online version of record will be different from this version once it has been copyedited and typeset.
PLEASE CITE THIS ARTICLE AS DOI: 10.1063/5.0319029

extension of pump–probe by FLIM, or of FLIM by PP. From the PP perspective, the FLIM detection allows measurement of small volumes of dilute samples, enabling time-resolved measurements of complex, fragile or precious samples.[41] From the FLIM perspective, the PP introduces ultrafast time resolution, allowing resolution of otherwise too fast photoinduced dynamics such as local variations of excitonic structure and transport.[85] To conclude, we believe that PP-FLIM will find its applications in chemical physics, biophysics and beyond.

SUPPLEMENTARY MATERIAL

See the supplementary material for further information on the broadband supercontinuum generation of the white light probe in the photonic crystal fibre, the determination of zero pump–probe time delay, the chirp correction procedure and the aggregation observed in cresyl violet and oxonol VI.

ACKNOWLEDGEMENTS

This project has at the beginning received funding from the European Union's Horizon 2020 research and innovation programme under the Marie Skłodowska-Curie grant agreement No. 101030656. The authors acknowledge funding by Charles University (grant no. PRIMUS/24/SCI/007, to P.M.).

AUTHOR DECLARATIONS

Conflict of Interest: The authors have no conflicts to disclose.

AUTHOR CONTRIBUTIONS

M. Garrow: Data Curation (lead); Formal analysis (equal); Investigation (equal); Software (equal); Visualization (lead); Writing/Original Draft Preparation (lead); Writing/Review & Editing (supporting). **A. Haboucha**: Resources (lead); Writing/Review & Editing (supporting). **P. Heřman**: Conceptualization (supporting); Project administration (equal); Resources (supporting); Writing/Review & Editing (supporting). **P. Malý**: Conceptualization (lead); Formal analysis (equal); Funding Acquisition (lead); Investigation (equal); Methodology (lead); Project administration (equal); Software (equal); Supervision (lead); Writing/Original Draft Preparation (supporting); Writing/Review & Editing (lead)

DATA AVAILABILITY

The data that support the findings of this study are available from the corresponding author upon reasonable request.

REFERENCES

1. Schuurman, M. S. & Blanchet, V. Time-resolved photoelectron spectroscopy: the continuing evolution of a mature technique. *Physical Chemistry Chemical Physics* vol. 24 20012–20024 (2022).

2. Fielding, H. H. & Worth, G. A. Using time-resolved photoelectron spectroscopy to

ACCEPTED MANUSCRIPT
The Journal of Chemical Physics
AIP Publishing
This is the author's peer reviewed, accepted manuscript. However, the online version of record will be different from this version once it has been copyedited and typeset.
PLEASE CITE THIS ARTICLE AS DOI: 10.1063/5.0319029

unravel the electronic relaxation dynamics of photoexcited molecules. *Chemical Society Reviews* vol. 47 309–321 (2018).

3. Townsend, D. Mapping extended reaction coordinates in photochemical dynamics. *J. Mol. Spectrosc.* **395**, 111807 (2023).

4. Berera, R., van Grondelle, R. & Kennis, J. T. M. Ultrafast transient absorption spectroscopy: Principles and application to photosynthetic systems. *Photosynth. Res.* **101**, 105–118 (2009).

5. Ghasemi, M., Lu, J., Jia, B. & Wen, X. Steady state and transient absorption spectroscopy in metal halide perovskites. *Chemical Society Reviews* vol. 54 1644–1683 (2025).

6. Dobryakov, A. L. *et al.* Femtosecond pump/supercontinuum-probe spectroscopy: Optimized setup and signal analysis for single-shot spectral referencing. *Rev. Sci. Instrum.* **81**, 113106 (2010).

7. Chen, Z. Q. *et al.* Lighting the Path to Practical Applications of Single-Atom Catalysts in Photocatalysis: The Role of Platinum Group Single Atoms in Enhancing Catalytic Activity. *Solar RRL* vol. 9 (2025).

8. Sakizadeh, J. D., Weiss, R., Scholes, G. D. & Kudisch, B. Ultrafast Spectroscopy and Dynamics of Photoredox Catalysis. *Annu. Rev. Phys. Chem.* (2025) doi:10.1146/annurev-physchem-082423.

9. Bakulin, A. A., Silva, C. & Vella, E. Ultrafast Spectroscopy with Photocurrent Detection: Watching Excitonic Optoelectronic Systems at Work. *J. Phys. Chem. Lett.* **7**, 250–258 (2016).

10. Shaheen, B. S. *et al.* Real-Space Mapping of Surface-Oxygen Defect States in Photovoltaic Materials Using Low-Voltage Scanning Ultrafast Electron Microscopy. *ACS Appl. Mater. Interfaces* **12**, 7760–7767 (2020).

11. Hancock, A. M. *et al.* Ultrafast energy transfer between lipid-linked chromophores and plant light-harvesting complex II. *Phys. Chem. Chem. Phys.* **23**, 19511–19524 (2021).

12. Barcus, K. *et al.* Charge transfer in hybrid quantum dot / metal-organic framework systems: Current understanding and future challenges. *Coordination Chemistry Reviews* vol. 542 (2025).

13. Jahan, I., Harun-Ur-Rashid, M., Almuhayawi, M. S., Al Jaouni, S. K. & Selim, S. Emerging ultrafast technologies in biotechnology. *3 Biotech* vol. 15 (2025).

14. Zigmantas, D., Polívka, T., Persson, P. & Sundström, V. Ultrafast laser spectroscopy uncovers mechanisms of light energy conversion in photosynthesis and sustainable energy materials. *Chem. Phys. Rev.* **3**, (2022).

15. Christensson, N. *et al.* Origin of the bathochromic shift of astaxanthin in lobster protein: 2D electronic spectroscopy investigation of β-crustacyanin. *J. Phys. Chem. B* **117**, 11209–11219 (2013).

16. Polívka, T. & Sundström, V. Ultrafast dynamics of carotenoid excited states-from solution to natural and artificial systems. *Chem. Rev.* **104**, 2021–2071 (2004).

ACCEPTED MANUSCRIPT
The Journal of Chemical Physics
AIP Publishing
This is the author's peer reviewed, accepted manuscript. However, the online version of record will be different from this version once it has been copyedited and typeset.
PLEASE CITE THIS ARTICLE AS DOI: 10.1063/5.0319029

17. Fleming, G. R. & Cho, M. Chromophore-solvent dynamics. **47**, 109–134.

18. Rosspeintner, A., Lang, B. & Vauthey, E. Ultrafast photochemistry in liquids. *Annu. Rev. Phys. Chem.* **64**, 247–271 (2013).

19. Zhang, X., Lefebvre, P. L. & Harvey, J. N. Effect of solvent motions on the dynamics of the Diels–Alder reaction. *Phys. Chem. Chem. Phys.* **24**, 1120–1130 (2022).

20. Kovalenko, S. A., Dobryakov, A. L., Ruthmann, J. & Ernsting, N. P. Femtosecond spectroscopy of condensed phases with chirped supercontinuum probing. *Phys. Rev. A - At. Mol. Opt. Phys.* **59**, 2369–2384 (1999).

21. Dietzek, B., Pascher, T., Sundström, V. & Yartsev, A. Appearance of coherent artifact signals in femtosecond transient absorption spectroscopy in dependence on detector design. *Laser Phys. Lett.* **4**, 38–43 (2007).

22. Lorenc, M. *et al.* Artifacts in femtosecond transient absorption spectroscopy. *Appl. Phys. B Lasers Opt.* **74**, 19–27 (2002).

23. Deng, J., Gong, N. & Ma, L. Capturing Ultrafast Carrier and Exciton Transport: Advances in Wide-Field Transient Absorption Microscopy. *J. Phys. Chem. Lett.* **16**, 11183–11195 (2025).

24. Fischer, M. C., Wilson, J. W., Robles, F. E. & Warren, W. S. Invited Review Article: Pump-probe microscopy. *Rev. Sci. Instrum.* **87**, 31101 (2016).

25. Malý, P. & Brixner, T. Fluorescence-Detected Pump–Probe Spectroscopy. *Angew. Chemie - Int. Ed.* **60**, 18867–18875 (2021).

26. Hao, H. *et al.* Fluorescence-Detected Pump-Probe Spectroscopy for Artifact-Free Detection of Stokes Shift Dynamics. *J. Phys. Chem. Lett.* **16**, 4861–4868 (2025).

27. Fersch, D. *et al.* Single-Molecule Ultrafast Fluorescence-Detected Pump-Probe Microscopy. *J. Phys. Chem. Lett.* **14**, 4923–4932 (2023).

28. Cho, M. *Two-dimensional optical spectroscopy*. (CRC Press).

29. Tiwari, V. *et al.* Spatially-resolved fluorescence-detected two-dimensional electronic spectroscopy probes varying excitonic structure in photosynthetic bacteria. *Nat. Commun.* **9**, 4219 (2018).

30. Tekavec, P. F., Lott, G. A. & Marcus, A. H. Fluorescence-detected two-dimensional electronic coherence spectroscopy by acousto-optic phase modulation. *J. Chem. Phys.* **127**, 214307 (2007).

31. Draeger, S., Roeding, S. & Brixner, T. Rapid-scan coherent 2D fluorescence spectroscopy. *Opt. Express* **25**, 3259 (2017).

32. De, A. K., Monahan, D., Dawlaty, J. M. & Fleming, G. R. Two-dimensional fluorescence-detected coherent spectroscopy with absolute phasing by confocal imaging of a dynamic grating and 27-step phase-cycling. *J. Chem. Phys.* **140**, 1–9 (2014).

33. Lakowitz, J. R. *Principles of Fluorescence Spectroscopy*. (Springer Science & Business Media, 2013).

ACCEPTED MANUSCRIPT
The Journal of Chemical Physics
AIP Publishing
This is the author's peer reviewed, accepted manuscript. However, the online version of record will be different from this version once it has been copyedited and typeset.
PLEASE CITE THIS ARTICLE AS DOI: 10.1063/5.0319029

34. Ali, F. & Kundu, S. Fluorescence Lifetime Imaging Microscopy: Advances in Materials Science Research. *Chem. Mater.* **37**, 3903–3926 (2025).

35. Berezin, M. Y. & Achilefu, S. Fluorescence Lifetime Measurements and Biological Imaging. *Chem. Rev.* **110**, 2641–2684 (2010).

36. Suhling, K., French, P. M. W. & Phillips, D. Time-resolved fluorescence microscopy. *Photochem. Photobiol. Sci.* **4**, 13–22 (2005).

37. Jares-Erijman, E. A. & Jovin, T. M. FRET imaging. *Nat. Biotechnol.* **21**, 1387–1395 (2003).

38. Strachotová, D., Holoubek, A., Wolfová, K., Brodská, B. & Heřman, P. Cytoplasmic localization of Mdm2 in cells expressing mutated <scp>NPM</scp> is mediated by p53. *FEBS J.* **290**, 4281–4299 (2023).

39. Malý, P., Strachotová, D., Holoubek, A. & Heřman, P. Interferometric excitation fluorescence lifetime imaging microscopy. *Nat. Commun.* **15**, 8019 (2024).

40. Jonas, D. M. Two-dimensional femtosecond spectroscopy. *Annu. Rev. Phys. Chem.* **54**, 425–463 (2003).

41. Gross, N. *et al.* Progress and Prospects in Optical Ultrafast Microscopy in the Visible Spectral Region: Transient Absorption and Two-Dimensional Microscopy. *Journal of Physical Chemistry C* vol. 127 14557–14586 (2023).

42. Ostovar, B. *et al.* Acoustic Vibrations of Al Nanocrystals: Size, Shape, and Crystallinity Revealed by Single-Particle Transient Extinction Spectroscopy. *J. Phys. Chem. A* **124**, 3924–3934 (2020).

43. Réhault, J. *et al.* 2D IR spectroscopy with phase-locked pulse pairs from a birefringent delay line. *Opt. Express* **22**, 123107 (2014).

44. Brida, D., Manzoni, C. & Cerullo, G. Phase-locked pulses for two-dimensional spectroscopy by a birefringent delay line. *Opt. Lett.* **37**, 3027–3029 (2012).

45. Borrego-Varillas, R. *et al.* Two-dimensional electronic spectroscopy in the ultraviolet by a birefringent delay line. *Opt. Express* **24**, 28491–28499 (2016).

46. Upputuri, P. K. & Pramanik, M. Microsphere-aided optical microscopy and its applications for super-resolution imaging. *Opt. Commun.* **404**, 32–41 (2017).

47. Smith, J. C., Hallidy, L. & Topp, M. R. The Behavior of the Fluorescence Lifetime and Polarization of Oxonol Potential-Sensitive Extrinsic Probes in Solution and in Beef Heart Submitochondrial Particles. *J. Membr. Biol.* **60**, 173–185 (1981).

48. Das, N. K., Ghosh, S., Jaiswal, S., Tewary, A. & Mukherjee, S. Micelles entrapped Cresyl Violet can selectively detect copper and mercury ions in solution: A fluorescence Correlation Spectroscopy investigation. *Chem. Phys. Lett.* **682**, 147–153 (2017).

49. van Stokkum, I. H. M., Larsen, D. S. & van Grondelle, R. Global and target analysis of time-resolved spectra. *Biochim. Biophys. Acta - Bioenerg.* **1657**, 82–104 (2004).

50. Ishii, K. & Tahara, T. Two-dimensional fluorescence lifetime correlation spectroscopy. 2. Application. *J. Phys. Chem. B* **117**, 11423–11432 (2013).

ACCEPTED MANUSCRIPT
The Journal of Chemical Physics
AIP Publishing
This is the author's peer reviewed, accepted manuscript. However, the online version of record will be different from this version once it has been copyedited and typeset.
PLEASE CITE THIS ARTICLE AS DOI: 10.1063/5.0319029

51. Jafari, A., Ghanadzadeh, A., Tajalli, H., Yeganeh, M. & Moghadam, M. Electronic absorption spectra of cresyl violet acetate in anisotropic and isotropic solvents. *Spectrochim. Acta - Part A Mol. Biomol. Spectrosc.* **66**, 717–725 (2007).

52. Takeshita, T. Effect of the TiO2 surface modification with 3-glycidyloxypropyltrimethoxysilane on the aggregation of cresyl violet: Application to a dye-sensitized solar cell. *Mater. Chem. Phys.* **286**, 126196 (2022).

53. Kostjukov, V. V. Photoexcitation of cresyl violet dye in aqueous solution: TD-DFT study. *Theor. Chem. Acc.* **140**, (2021).

54. Bashford, C. L. & Thayer, W. S. Thermodynamics of the electrochemical proton gradient in bovine heart submitochondrial particles. *J. Biol. Chem.* **252**, 8459–8463 (1977).

55. Leng, W. & Kelley, A. M. Resonance Raman intensity analysis of cresyl violet bound to SiO 2 colloidal nanoparticles. *Langmuir* **19**, 7049–7055 (2003).

56. Steinhurst, D. A. & Owrutsky, J. C. Second harmonic generation from oxazine dyes at the air/water interface. *J. Phys. Chem. B* **105**, 3062–3072 (2001).

57. Banik, S., Hussain, S. A. & Bhattacharjee, D. Modified aggregation pattern of cresyl violet acetate adsorbed on nano clay mineral layers in Langmuir Blodgett film. *J. Photochem. Photobiol. A Chem.* **353**, 570–580 (2018).

58. Cao, S. *et al.* Ultrafast Fluorescence Spectroscopy via Upconversion and Its Applications in Biophysics. *Molecules* **26**, 211 (2021).

59. Petushkov, V. N. *et al.* Ultrafast Fluorescence Relaxation Spectroscopy of 6,7-Dimethyl-(8-ribityl)-lumazine and Riboflavin, Free and Bound to Antenna Proteins from Bioluminescent Bacteria. *J. Phys. Chem. B* **107**, 10934–10939 (2003).

60. Lakowicz, J. R. *Principles of Fluorescence Spectroscopy*. (Springer, 2006).

61. Krishnamurthy, M., Khan, K. K. & Doraiswamy, S. Rotational diffusion kinetics of polar solutes in hexamethylphosphoramide- water systems. *J. Chem. Phys.* **98**, 8640–8646 (1993).

62. Liu, D. & Kamat, P. V. Picosecond dynamics of cresyl violet H-aggregates adsorbed on SiO2 and SnO2 nanocrystallites. *J. Chem. Phys.* **105**, 965–970 (1996).

63. Blankenship, R. E. *Molecular mechanisms of photosynthesis, 2nd edition*. (Wiley-Blackwell, 2014).

64. Wientjes, E., van Amerongen, H. & Croce, R. LHCII is an antenna of both photosystems after long-term acclimation. *Biochim. Biophys. Acta - Bioenerg.* **1827**, 420–426 (2013).

65. Wientjes, E., Philippi, J., Borst, J. W. & van Amerongen, H. Imaging the Photosystem I/Photosystem II chlorophyll ratio inside the leaf. *Biochim. Biophys. Acta - Bioenerg.* **1858**, 259–265 (2017).

66. Xu, S. *et al.* Ultrafast spectroscopy studies on the mechanism of electron transfer and energy conversion in the isolated pseudo ginseng, water hyacinth and spinach chloroplasts. *Sci. China, Ser. B Chem.* **44**, 366–380 (2001).

ACCEPTED MANUSCRIPT
The Journal of Chemical Physics
AIP Publishing
This is the author's peer reviewed, accepted manuscript. However, the online version of record will be different from this version once it has been copyedited and typeset.
PLEASE CITE THIS ARTICLE AS DOI: 10.1063/5.0319029

67. Iermak, I., Vink, J., Bader, A. N., Wientjes, E. & van Amerongen, H. Visualizing heterogeneity of photosynthetic properties of plant leaves with two-photon fluorescence lifetime imaging microscopy. *Biochim. Biophys. Acta - Bioenerg.* **1857**, 1473–1478 (2016).

68. Connolly, J. S., Janzen, A. F. & Samuel, E. B. Fluorescence lifetimes of chlorophyll a: solvent, concentration and oxygen dependence. *Photochem. Photobiol.* **36**, 559–563 (1982).

69. Bolzonello, L., Bruschi, M., Fresch, B. & van Hulst, N. F. Nonlinear Optical Spectroscopy of Molecular Assemblies: What Is Gained and Lost in Action Detection? *J. Phys. Chem. Lett.* **14**, 11438–11446 (2023).

70. Moriwaki, T. *et al.* Chloroplast and outside-chloroplast interference of light inside leaves. *Environ. Exp. Bot.* **208**, 105258 (2023).

71. Valkunas, L., Trinkunas, G., Liuolia, V. & van Grondelle, R. Nonlinear annihilation of excitations in photosynthetic systems. *Biophys J* **69**, 1117–29 (1995).

72. McNamee, M. G. *et al.* Uncovering Transport Mechanisms in Perovskite Materials and Devices with Recombination-Induced Action Spectroscopies. *J. Phys. Chem. C* **127**, 2782–2791 (2023).

73. Grégoire, P. *et al.* Incoherent population mixing contributions to phase-modulation two-dimensional coherent excitation spectra. *J. Chem. Phys.* **147**, 114201 (2017).

74. Charvátová, K. & Malý, P. Spectro-temporal symmetry in action-detected optical spectroscopy: Highlighting excited-state dynamics in large systems. *J. Chem. Phys.* **162**, 124204 (2025).

75. Perri, A. *et al.* Excitation-Emission Fluorescence Spectroscopy with Single Molecule Sensitivity Using a Common-Path Interferometer. in *Light, Energy and the Environment 2018 (E2, FTS, HISE, SOLAR, SSL)* FT3B.5 (Optical Society of America, 2018). doi:10.1364/FTS.2018.FT3B.5.

76. Wang, Z., Lei, S., Karki, K. J., Jakobsson, A. & Pullerits, T. Compressed Sensing for Reconstructing Coherent Multidimensional Spectra. *J. Phys. Chem. A* **124**, 1861–1866 (2020).

77. Bolzonello, L., van Hulst, N. F. & Jakobsson, A. Fisher information for smart sampling in time-domain spectroscopy. *J. Chem. Phys.* **160**, (2024).

78. Wilson, T. & Sheppard, C. *Theory and Practice of Scanning Optical Microscopy*. *Academic Press* (1985). doi:10.1364/josaa.4.000551.

79. Miyazaki, J., Kawasumi, K. & Kobayashi, T. Resolution improvement in laser diode-based pump–probe microscopy with an annular pupil filter. *Opt. Lett.* **39**, 4219–4222 (2014).

80. Ronceray, N. *et al.* Wide-field fluorescence lifetime imaging of single molecules with a gated single-photon camera. *Light Sci. Appl.* **14**, 258 (2025).

81. Lang, B. Photometrics of ultrafast and fast broadband electronic transient absorption spectroscopy: State of the art. *Rev. Sci. Instrum.* **89**, 93112 (2018).

ACCEPTED MANUSCRIPT
The Journal of Chemical Physics
AIP Publishing
This is the author's peer reviewed, accepted manuscript. However, the online version of record will be different from this version once it has been copyedited and typeset.
PLEASE CITE THIS ARTICLE AS DOI: 10.1063/5.0319029

82. Li, H. *et al.* Ultrahigh sensitive transient absorption spectrometer. *Rev. Sci. Instrum.* **92**, 53002 (2021).

83. Lang, B. *et al.* Broadband ultraviolet-visible transient absorption spectroscopy in the nanosecond to microsecond time domain with sub-nanosecond time resolution. *Rev. Sci. Instrum.* **84**, 73107 (2013).

84. Maiuri, M., Garavelli, M. & Cerullo, G. Ultrafast Spectroscopy: State of the Art and Open Challenges. *J. Am. Chem. Soc.* **142**, 3–15 (2020).

85. Hoang, N. V., Nikolis, V. C., Baisinger, L., Vandewal, K. & Pshenichnikov, M. S. Diffusion-enhanced exciton dissociation in single-material organic solar cells. *Phys. Chem. Chem. Phys.* **23**, 20848–20853 (2021).